Dual partitioning and attachment effects of rhamnolipid on pyrene biodegradation under bioavailability restrictions

Eleonora Congiu[1], John R. Parsons[2] and José-Julio Ortega-Calvo[1,*]

[1]*Instituto de Recursos Naturales y Agrobiología (IRNAS), C.S.I.C., Apartado 1052, E-41080-Seville, Spain*

[2]*Institute for Biodiversity and Ecosystem Dynamics (IBED), University of Amsterdam, 94248, Amsterdam, 1092 GE, The Netherlands*

*Address correspondence to Jose Julio Ortega-Calvo, jjortega@irnase.csic.es.

July 1, 2015

ABSTRACT

We investigated the effects of different bioavailability scenarios on the rhamnolipid-enhanced biodegradation of pyrene by the representative polycyclic aromatic hydrocarbon degrader *Mycobacterium gilvum* VM552. This biosurfactant enhanced biodegradation when pyrene was provided in the form of solid crystals; no effect was observed when the same amount of the chemical was preloaded on polydimethylsiloxane (PDMS). An enhanced effect was observed when pyrene was sorbed into soil but not with the dissolved compound. Synchronous fluorescence spectrophotometry and liquid scintillation were used to determine the phase exchange of pyrene. We also investigated the phase distribution of bacteria. Our results suggest that the rhamnolipid can enhance the biodegradation of pyrene by micellar solubilization and diffusive uptake. These mechanisms increase substrate acquisition by bacterial cells at exposure concentrations well above the half-saturation constant for active uptake. The moderate solubilization of pyrene from PDMS by the rhamnolipid and the prevention of cell attachment may explain the lack of enhancement for pyrene-preloaded PDMS.

Keywords: Biodegradation, Pyrene, Dissolution, Rhamnolipid, Biosurfactant, Synchronous fluorescence

Capsule abstract:

Rhamnolipid-enhanced biodegradation of pyrene may depend on the exposure regime. Moderate solubilization from difficult matrices and prevention of cell attachment may have no effect.

1. Introduction

Polycyclic aromatic hydrocarbons (PAHs) are ubiquitous organic contaminants and may have potentially harmful effects toward human health and the environment. Biodegradation is a key factor in the environmental impact of these hydrophobic organic compounds and is often the basis for the sustainable remediation of contaminated soils and sediments. However, a successful bioremediation is often limited by the low bioavailability of these chemicals. PAHs tend to strongly sorb to solid surfaces but desorb slowly. This slow desorption is often the limiting factor in biodegradation (Johnsen et al., 2005; Yang et al., 2011).

A promising strategy to improve the bioavailability of soil-sorbed PAHs is the use of biosurfactants. In recent decades, biosurfactants have become known as environmentally benign alternatives to chemical surfactants (Banat et al., 2010). The anionic, rhamnolipid biosurfactant produced by *Pseudomonas aeruginosa* is one of the most studied biosurfactants. This biosurfactant can enhance the biodegradation of PAHs by increasing the dissolution rate of crystalline chemicals (Zhang et al., 1997) in nonaqueous-phase liquids (NAPLs) (Garcia-Junco et al., 2003) and when sorbed into soils (Congiu and Ortega-Calvo, 2014). New approaches are required to enhance the bioavailability of PAHs through biosurfactants in a cost-effective manner without exceeding regulatory concentration levels (Ortega-Calvo et al., 2013). In contaminated soils, the efficiency of biosurfactants for bioremediation is dependent on the physicochemical environment of the soil, the mass transfer rate, and the balance between the solubilization of the chemical and the sorption of the biosurfactant to the soil (Ochoa-Loza and Noordman, 2007). The successful application of biosurfactants should also minimize the risks associated with the increased chemical activity and toxicity of the PAHs and metabolites as a result of solubilization at concentrations in excess of the metabolic potential of microorganisms. These concentrations may be high compared with the affinity constant (K_m) of microbial enzymes and uptake mechanisms, thus saturating the

63 biodegradation process. This effect may be relevant during the treatment of point-source PAH
64 pollution in soils and sediments, which typically have high pollutant concentrations and a wide
65 diversity of desorption patterns (Cornelissen et al., 1998; Gomez-Lahoz and Ortega-Calvo, 2005;
66 Rhodes et al., 2010).

67 Biodegradable chemical surfactants can enhance bioremediation in soils where biodegradation
68 has already removed the fast-desorbing PAHs, leaving the slowly desorbing residue (Bueno-Montes
69 et al., 2011; Zhu and Aitken, 2010). The environmentally friendly advantage of rhamnolipids over
70 chemical surfactants is of considerable interest in applications for removing slowly desorbing
71 PAHs. However, the removal of slowly desorbing pollutants via biosurfactants is limited. For
72 example, rhamnolipid efficiency may decrease as a result of intra-aggregate diffusion limitations on
73 the solubilization process due to pollutant aging (Congiu and Ortega-Calvo, 2014). Rhamnolipids
74 may also have antiadhesive activity toward bacteria (Nickzad and Deziel, 2014) and may negatively
75 impact the biodegradation of PAHs because, under bioavailability restrictions, adherent bacteria
76 have better access to hydrophobic pollutants than suspended bacteria (Ortega-Calvo and Alexander,
77 1994). Few studies have examined the solubilizing effect of rhamnolipids on PAHs for different
78 levels of chemical activity and on bacterial attachment to the pollutant source.

79 Therefore, the aim of this study was to investigate the effects of different exposure scenarios
80 that result in dissimilar phase exchanges of pyrene on rhamnolipid-enhanced biodegradation. The
81 scenarios used in this study were designed to create wide changes in the exposure concentrations of
82 the contaminant. Therefore, the effect of the rhamnolipid on the biodegradation of pyrene by a
83 representative PAH degrading bacterium, *Mycobacterium gilvum* VM552, was tested with systems
84 in which the chemical was supplied either completely dissolved in an aqueous solution, sorbed to
85 soil, in its crystalline form or partitioned into a preloaded silicone polymer. This partitioning-based
86 method enabled the study of the biotransformation kinetics of hydrophobic organic chemicals under
87 controlled conditions (Smith et al., 2012). The aim was to generate different bioavailability

restrictive conditions that involved dissimilar dissolution rates and aqueous phase concentrations, taking as a reference the half-saturation affinity constant for the bacterial uptake of the dissolved compound. We also investigated the phase distribution of bacterial cells in our experimental systems.

2. Experimental section

2.1. Chemicals

^{14}C-pyrene (58.8 mCi/mmol, radiochemical purity >98%) was purchased from Campro Scientific GmbH (Veenendaal, The Netherlands). Unlabeled phenanthrene and pyrene were obtained from Sigma-Aldrich (Madrid, Spain). Analytical grade hexane and acetone were supplied by Panreac (Barcelona, Spain). Polydimethylsiloxane (Silastic MDX4-4210 BioMedical Grade Elastomer Kit) was purchased from Dow Corning Corporation (Midland, MI).

2.2. Bacteria, media, and cultivation

Pseudomonas aeruginosa 19SJ, a strain originally isolated from a petroleum-contaminated soil, was selected as the rhamnolipid biosurfactant producer. The strain was routinely maintained in a liquid SWF medium containing 2% (w/v) mannitol as the sole source of carbon (Garcia-Junco et al., 2003).

Mycobacterium gilvum VM552, a strain able to grow with phenanthrene and pyrene, was used as the inoculum for mineralization experiments. The strain was cultured with phenanthrene as the sole source of carbon and prepared for mineralization experiments in an inorganic salt solution (mineralization medium, MM) as previously described (Bueno-Montes et al., 2011). To prevent

113 the precipitation of the rhamnolipid, the pH of the solution was adjusted to 6.7 with 0.05 M sodium
114 bicarbonate.
115
116 *2.3. Biosurfactant*
117
118 The rhamnolipid biosurfactant produced by *P. aeruginosa* 19SJ was purified and quantified
119 following procedures previously described (Congiu and Ortega-Calvo, 2014). The biosurfactant is
120 composed mainly of L-rhamnosyl-3-hydroxydecanoyl-3-hydroxydecanoate and L-rhamnosyl-L-
121 rhamnosyl-3-hydroxy-decanoyl-3-hydroxydecanoate, besides a small proportion of other congeners
122 with variable length-hydrocarbon chains (C10−C18). The final rhamnolipid concentration was
123 quantified as rhamnose equivalents (RE) by the orcinol method. The surface tension of the
124 rhamnolipid solutions (in MM) was estimated at 23 ºC with a TD1 Lauda ring tensiometer. In our
125 conditions, the critical micelle concentration (CMC) of the biosurfactant was 40 mg/L.
126
127 *2.4. Sorption onto soil, desorption and solubilization*
128
129 The sorption of ^{14}C-labeled pyrene onto soil was achieved using a procedure previously
130 described (Congiu and Ortega-Calvo, 2014) and adapted to create different exposure
131 concentrations. The soil sample used in this study was a sandy-loam forest soil originating from Los
132 Alcornocales Natural Park (Cádiz, Spain) with 6.1% organic matter and 5.5% clay. The background
133 concentration of pyrene in the soil was 66 µg/kg, which was present in a highly recalcitrant form
134 (Posada-Baquero and Ortega-Calvo, 2011). Briefly, 16 mg of dry soil was introduced into 50-mL
135 glass bottles (Schott), together with 10 mL MM containing 8.4 ng/mL dissolved ^{14}C-pyrene (5,000
136 dpm/mL). The bottles were incubated for 24 h. This contact period was sufficient to cause
137 restrictions for the biodegradation of the soil-sorbed pyrene (Congiu and Ortega-Calvo, 2014). The

concentration of ^{14}C-pyrene in the aqueous solution was determined after centrifugation, by radioactivity measurements using a liquid scintillation counter (Model LS6500, Beckman) while the concentration of the sorbate was calculated by difference. Assuming that equilibrium was achieved after this contact period, the solid-water distribution, K_d (in L/kg) was calculated as previously described (Congiu and Ortega-Calvo, 2014). A theoretical K_d value was estimated from the organic carbon-normalized distribution coefficient (K_{oc}) for the compound (Schwarzenbach et al., 2003).

Desorption experiments with soil-sorbed pyrene were performed in soil suspensions with the Tenax solid-phase extraction method using a previously described procedure (Congiu and Ortega-Calvo, 2014). After selected time intervals, Tenax was separated from the soil suspensions and the same amount of fresh Tenax was added to repeat the cycle. The Tenax was extracted with acetone-hexane (1:1) for subsequent radioactivity measurements. This procedure was not possible with the rhamnolipid because of the interference of the biosurfactant foam on the recovery of the Tenax beads. Instead, the solubilization of sorbed pyrene in the presence of the rhamnolipid was determined by centrifugation of soil suspensions as described elsewhere (Congiu and Ortega-Calvo, 2014).

2.5. Dissolution of crystalline and polydimethylsiloxane-associated pyrene in the presence of rhamnolipid

The effects of the rhamnolipid on the dissolution of crystalline pyrene and pyrene-preloaded polydimethylsiloxane (PDMS) were studied using conditions comparable with those of the mineralization experiments but in the absence of bacteria (Tejeda-Agredano et al., 2014). To measure the dissolution of crystalline pyrene, an acetone solution of ^{14}C-pyrene (50,000 dpm) and of unlabeled pyrene to achieve a final concentration of 5 µg/mL, was evaporated at the bottom of 15-mL Pyrex tubes. Then, 5 mL of MM containing rhamnolipid (400 mg/mL) and bicarbonate was

163 added to the tubes. The experiments were performed in triplicate in a series of four tubes
164 maintained at 25 ºC on a rotary shaker operating at 80 rpm. At selected time intervals, 0.5 mL of a
165 homogeneous sample was taken directly from each tube. To determine the dissolved pyrene
166 concentrations, the samples were measured by synchronous fluorescence spectrophotometry (SFS)
167 with an F-2500 fluorescence spectrophotometer (Hitachi) as previously described (Ortega-Calvo
168 and Gschwend, 2010). Inner-filter effects on fluorescence quantifications with and without
169 biosurfactant were corrected by absorbances at 260 nm and 370 nm using a UV/visible
170 spectrophotometer (Lambda EZ210, Perkin Elmer). Liquid scintillation counting (LSC) was used
171 for parallel determinations of dissolved pyrene. Samples were transferred from quartz cuvettes to 6-
172 mL liquid scintillation vials and mixed with a 5 mL liquid scintillation cocktail. Then, the
173 radioactivity was determined with the scintillation counter.

174 Experiments with PDMS-associated pyrene were performed under conditions identical to
175 those described for crystalline pyrene but using 20-mL glass vials with 500 ± 5 mg of PDMS fixed
176 at the vial base and 5 mL of MM. The amount of pyrene per vial was the same as in the experiments
177 with the crystalline chemical. More details about the vial preparation can be found elsewhere
178 (Tejeda Agredano et al., 2014).

179

180 *2.6. Mineralization experiments*

181

182 Mineralization experiments of soil-sorbed ^{14}C-pyrene were performed with equilibrated soil
183 suspensions as described. Rhamnolipid (400 mg/L) and sodium bicarbonate were added to the
184 flasks with the bacterial inoculum, and the volume was brought to 20 mL with MM (to a final cell
185 density of approximately 5 x 10^8 cells/mL). The flasks were closed with Teflon-lined stoppers
186 equipped with a suspended 2-mL vial that contained 1 mL of 0.5 M NaOH and were maintained at
187 23 ± 2 ºC on an orbital shaker operating at 150 rpm. Then, ^{14}C-pyrene mineralization was measured

188 by the amount of $^{14}CO_2$ production in an alkali trap (Posada-Baquero and Ortega-Calvo, 2011).
189 Under the same conditions, control experiments with water-dissolved pyrene in the presence and
190 absence of the rhamnolipid biosurfactant were also run.

191 Mineralization experiments with crystalline and PDMS-associated pyrene were performed as
192 described above for the abiotic dissolution experiments (Tejeda Agredano et al., 2014). First, 5 mL
193 of MM containing the rhamnolipid (400 mg/L), sodium bicarbonate and the bacterial inoculum (in
194 MM, at a final density of 5 x 10^8 cell/mL) was added to 15-mL Pyrex tubes (crystalline pyrene
195 experiment) or 20-mL vials (PDMS-associated pyrene experiment). A glass rod (0.5 cm diameter
196 and 2 cm length) was used to facilitate mixing during incubation. The tubes were sealed with
197 Teflon-lined stoppers and maintained at 25 ºC on an orbital shaker operating at 80 rpm. The
198 remainder of the procedure is the same as that described earlier. Student's t-test (SPSS 18 program)
199 was used for statistical comparisons.

200

201 *2.7. Data analysis*

202

203 The desorption and mineralization data of soil-sorbed pyrene experiments were analyzed with
204 the equation:

205 $$S_t / S_0 = F_{fast}\, exp\,(-k_{fast}\, t) + F_{slow}\, exp\,(-k_{slow}\, t) \qquad (1)$$

206 where S_t (g) and S_0 (g) are the amounts of PAHs sorbed onto the soil at time t (h) and at the start of
207 the experiment, respectively; F_{fast} and F_{slow} are the fast and slow-desorbing fractions, respectively;
208 and k_{fast} and k_{slow} (h^{-1}) are the rate constants of fast and slow desorption, respectively. These
209 parameters were obtained by minimizing the cumulative squared residuals between the
210 experimental and calculated values of $\ln(S_t/S_0)$. The software used to determine these parameters
211 was Microsoft Excel 2003 (Solver option). The mineralization data were analyzed with the same
212 equation in which the model parameters represent the fast and slow biodegradation fractions, F'_{fast}

213 and F'_{slow}, respectively, and the rate constants of fast and slow biodegradation, k'_{fast} (h^{-1}) and k'_{slow} (h^{-1}). The maximum mineralization rate (ng/mL/h) was calculated as k'_{fast} x F'_{fast}. The maximum partitioning or dissolution rate was calculated by multiplying C_{eq} by k.

216 The dissolution of crystalline pyrene and the partitioning of pyrene dissolved in PDMS were described using a two-compartment model, $dC/dt = k(C_{eq} - C)$, where C and C_{eq} (ng/mL) are the pyrene concentrations in the aqueous phase at time t and equilibrium, respectively; k (h^{-1}) is the mass transfer first order rate constant and t is the time (h). Assuming that $C = 0$ when $t = 0$, $dC/dt = k(C_{eq})$ where

$$C = C_{eq}(1-e^{-kt}) \quad (2)$$

222 Because the rate is maximum when $C = 0$, the maximum partitioning or dissolution rates can be calculated by multiplying C_{eq} by k (Efroymson and Alexander, 1994).

224 A similar model to Equation 2 was used to assess the mineralization data of the soil-free experiments:

$$P = P_{max}(1-e^{-k't}) \quad (3)$$

227 where P and P_{max} (%) are the activity converted to $^{14}CO_2$ at time t and the overall extent of ^{14}C-pyrene mineralization, respectively; k' (h^{-1}) is the biodegradation rate constant and t is the time (h). The maximum mineralization rate was calculated by multiplying P_{max} by k' (Guerin and Boyd, 1992).

231

232 *2.8. Bacterial attachment to pyrene crystals and PDMS*

233

234 Bacterial suspensions with and without rhamnolipid were placed in tubes with crystalline pyrene or in vials with PDMS. Attachment was estimated by decreased absorbance values at 600 nm after 24 h of incubation on an orbital shaker operating at 80 rpm and 25 ºC.

237

3. Results

3.1. Effect of rhamnolipid on pyrene phase exchange

The dissolution experiments were performed without bacteria to determine the influence of the rhamnolipid on the phase exchange of pyrene from crystals and PDMS to the aqueous phase (Figs. 1A and 1B, respectively). The concentrations of dissolved pyrene were determined in these experiments by synchronous fluorescence spectrophotometry (SFS). The results indicated that the dissolution rate of pyrene crystals, calculated with Equation 2, significantly increased in the presence of the rhamnolipid (Table 1). The increases can be attributed to the solubilization of pyrene caused by biosurfactant micelles. The equilibrium concentration of dissolved pyrene (including the freely dissolved and the rhamnolipid micelle-associated compound) in the presence of the biosurfactant was ten times higher than that of the control. We observed that the C_{eq} value without biosurfactant, 240.5 ng/mL (Table 1), was greater than the solubility of pyrene in water, i.e., 130 ng/mL (Tejeda-Agredano et al., 2014). This difference may be attributed to the presence of sodium bicarbonate in the control solutions (Schlautman et al., 2004). As expected, when pyrene was provided in PDMS in the absence of the biosurfactant, the C_{eq} value was seven times lower than that in the presence of the crystalline chemical. This result reflected the lower chemical activity of the compound in PDMS (Tejeda-Agredano et al., 2014). The rate of partitioning followed the same trend (Fig. 1B and Table 1). The rhamnolipid promoted the phase exchange of pyrene in these conditions, as indicated by significant increases in the partitioning rate and C_{eq}. However, the extent of this enhancement was less apparent than that with pyrene crystals.

Independent LSC estimations were conducted to confirm that the SFS-measured aqueous concentrations of pyrene corresponded with the total pyrene concentration in the aqueous phase in

262 the presence of rhamnolipid. This accounted for the freely dissolved pyrene molecules and the
263 pyrene molecules incorporated into the biosurfactant micelles. The use of ^{14}C-labeled pyrene in
264 these experiments enabled parallel measurements by SFS and LSC (Ortega-Calvo and Gschwend,
265 2010; Tejeda-Agredano et al., 2014). The LSC-estimated C_{eq} for crystalline pyrene was 215.2 ±
266 29.4 ng/mL and 2289.4 ± 458.3 ng/mL for the control and the rhamnolipid-treated samples,
267 respectively. The LSC-estimated PDMS C_{eq} was 120.6 ± 1.8 ng/mL and 38.2 ± 5.8 ng/mL, with and
268 without rhamnolipid, respectively. The complete results from the phase exchange experiments are
269 shown in Fig. S1. These LSC results were in good agreement with the SFS results (Table 1), which
270 indicated that the micelle-incorporated pyrene molecules produced the same fluorescence intensity
271 as the freely dissolved pyrene. The unchanged SFS pyrene signal in rhamnolipid micelles differed
272 from the other analytical situations. The micelle media of several surfactants enhanced the SFS
273 signal of PAH molecules (Patra and Mishra, 2002), even caused signal losses resulting from the
274 sorption of the PAH molecule to suspended sediment particles (Accardi-Dey and Gschwend, 2002),
275 bacterial cells (Ortega-Calvo and Gschwend, 2010) and dissolved humic acids (Tejeda-Agredano et
276 al., 2014).

277 In the absence of biosurfactant, the phase exchange from crystalline and PDMS-associated
278 pyrene resulted in C_{eq} values that were significantly greater than the K_m value (1.2 ng/mL) for
279 pyrene uptake by the bacterial strain used in this study. In another study that investigated oxygen
280 and sorption limitations for pyrene biodegradation in resuspension events and intact sediment beds,
281 the K_m was determined using pyrene exposure concentrations of up to 8 ng/mL (Ortega-Calvo and
282 Gschwend, 2010). In our study, sub-K_m exposure concentrations could have been achieved by using
283 PDMS loaded with a lower amount of pyrene. However, the results from the cell attachment
284 experiments (see section 3.3) showed a high affinity of cells to the PDMS surface. Due to the low
285 affinity of bacteria for particles from an organic matter-rich forest soil (Jimenez-Sanchez et al.,
286 2015), to avoid the interferences of cell attachment to the silicone reservoir during the

biodegradation of low concentrations of pyrene (Smith et al., 2012), we used the sorption properties of this soil to create different exposure scenarios with dissolved concentrations lower than K_m.

After the equilibration of the soil suspensions, the concentration of dissolved pyrene decreased from 4.2 ng/mL to 0.85 ± 0.06 ng/mL. The experimental and estimated log K_d for the sorption of pyrene showed similar values (3.7 and 3.3, respectively), which confirmed that soil organic carbon was the main factor responsible for pyrene sorption. The kinetics of desorption was determined under abiotic conditions by Tenax desorption. The desorption rate (Table 1) was significantly lower than the rates of phase exchange determined with crystalline and PDMS-associated pyrene. The kinetic analysis of solubilization in the presence of biosurfactant was not possible due to foam interference during Tenax beads separation. However, solubilization experiments showed that after 24 h, the concentration of pyrene in the aqueous phase in the presence of the rhamnolipid was approximately five times higher than the control without biosurfactant (Table 1). Furthermore, the dissolved pyrene concentration (0.5 ng/mL) was also lower than the K_m. Therefore, our primary hypothesis, which was based on the dependence of biosurfactant action on different exposure conditions, could be validated.

3.2. Effect of rhamnolipid on biodegradation of crystalline, PDMS-associated and sorbed pyrene

The rate of mineralization of pyrene (4.2 ng/mL) completely dissolved in the aqueous phase was not significantly different in the presence of rhamnolipid (0.5 ± 0.1 ng/mL/h) than in the biosurfactant-free control (0.4 ± 0.0 ng/mL/h). However, the rate of mineralization of crystalline pyrene (5 µg/mL) increased significantly in the presence of the rhamnolipid (Fig. 2A and Tables 1 and S1). The differences can be attributed to dissimilar k' values because the P_{max} values were not different (Equation 3). When the same amount of pyrene was provided in PDMS, no significant differences in mineralization rates were observed with and without biosurfactant (Table 1 and Fig.

312 2B). The maximum rate of biodegradation in the biosurfactant-free controls was not different
313 between crystalline pyrene and pyrene supplied by passive dosing (11.3 ng/mL/h and 16.8 ng/mL/h,
314 respectively). However, the mineralization curves (Figs. 2A and B) and the calculated P_{max} values
315 (79.1% and 38.4% for crystalline and PDMS-associated pyrene, respectively; see Table S1)
316 indicated that passive dosing halved the total amount of substrate transformed into CO_2.

317 The results from biodegradation experiments with soil-sorbed pyrene (S/W ratio 800 mg/L) in
318 the presence of rhamnolipid are shown in Fig. 2C. The maximum mineralization rate in the
319 biosurfactant-free control was substantially reduced compared with the crystalline and PDMS-
320 associated pyrene in accordance with the lower total concentration of pyrene in the system (Table
321 1). This rate was also lower than the rate determined in the soil-free controls that contained the
322 same amount of pyrene in the dissolved state as in the soil suspensions; this indicated desorption-
323 limiting conditions for biodegradation. These results show that the transformation was significantly
324 enhanced in the presence of the rhamnolipid. The enhancement was apparent through increases in
325 the fast biodegradation fraction (F'_{fast}) and its rate constant, k'_{fast} (Table S1).

326

327 *3.3. Dual partitioning and attachment effects of rhamnolipid on biodegradation*

328

329 Dissolution experiments with crystalline pyrene showed that with and without the
330 rhamnolipid, the aqueous-phase pyrene concentrations were well above K_m. Therefore, enhanced
331 biodegradation rates would not have been expected. To confirm biodegradation still allowed for the
332 removal of these high aqueous-phase concentrations in the presence of the rhamnolipid, we
333 measured dissolved pyrene in these bacterial suspensions with SFS, as shown in Fig. 3. These
334 results were compared with the abiotic dissolution data and the mineralization results during the
335 period in which the concentration of aqueous-phase pyrene was monitored. During the initial period
336 of maximum mineralization (approximately the first 30 h), bacterial cells were exposed to very high

337 concentrations of dissolved pyrene, similar to those determined in abiotic conditions. After this
338 period, the dissolved pyrene concentration decreased due to consumption but remained above K_m.
339 At these later stages, a corresponding decrease in the solid surface area available for pyrene
340 dissolution was likely occurring. This agrees with the high percentage (i.e., 25%) of substrate
341 mineralized after 45 h.

342 Pyrene may be more readily accessible to attached bacteria than suspended bacteria. This
343 enhances the mineralization rates under bioavailability restrictions (Ortega-Calvo and Alexander,
344 1994; Tejeda-Agredano et al., 2014). Therefore, we investigated bacterial attachment to pyrene
345 crystals and to pyrene-loaded PDMS in the presence and absence of the rhamnolipid. Bacterial
346 attachment to the crystals after 24 h was not affected by the presence of the rhamnolipid (34.8 ±
347 4.2%) when compared with the control (37.1 ± 4.6%). However, attachment to PDMS in the
348 presence of the rhamnolipid was 28.7 ± 5.9%, a value significantly lower than that of the control
349 (50.9 ± 1.1%). The reasons for the differences in the attachment to crystals and PDMS remain
350 unknown but may be related to differences in the interaction mechanisms between cell surfaces and
351 the hydrophilic and hydrophobic moieties of the biosurfactant and the solids (Stelmack et al., 1999).
352 These results indicate that the rhamnolipid in the PDMS system solubilized pyrene and also
353 significantly reduced the number of bacteria attached at the PDMS/water interface.
354

355 ## 4. Discussion

356

357 This study compared the effects of a rhamnolipid biosurfactant on the biodegradation of
358 dissimilar bioavailability scenarios resulting in the phase exchange of pyrene in three different
359 states: crystalline, partitioned into PDMS, and sorbed onto soil particles. The rhamnolipid enhanced
360 the biodegradation in the soil-sorbed and crystalline pyrene, whereas no effect was observed with

361 the PDMS-associated pyrene. The enhanced solubilization of the former two states likely increased
362 the biodegradation. Although the role of desorption kinetics in the rhamnolipid-enhanced
363 biodegradation of sorbed PAHs has been examined (Congiu and Ortega-Calvo, 2014), the aim of
364 our study was to determine whether rhamnolipid-enhanced biodegradation occurs over a broader
365 range of uptake scenarios. The observed enhancement of the biodegradation of the soil-sorbed
366 pyrene correlated with the solubilization results (Table 1), which show that dissolved pyrene
367 concentrations were lower than the K_m in the absence of the rhamnolipid. At this concentration
368 range, the uptake rates are directly related to the aqueous-phase concentrations of the substrates.
369 Because the bacterial cells were able to consume the biosurfactant micelle-partitioned pyrene as
370 rapidly as the solubilized pyrene, the rhamnolipid-induced micellar solubilization resulted in higher
371 biodegradation rates due to the exposure to a higher steady-state concentration of total pyrene in the
372 aqueous phase (Congiu and Ortega-Calvo, 2014).

373 However, the increased biodegradation observed with crystalline pyrene cannot be explained
374 by the same mechanisms as the soil suspensions because the exposure concentrations were at
375 saturating levels during the uptake. In the absence of the biosurfactant, the rate of dissolution of
376 crystalline pyrene was higher than the rate of biodegradation (Table 1). Therefore, the dissolution
377 rate was not a limiting factor for biodegradation. In the presence of the biosurfactant, we confirmed
378 through SFS measurements in bacterial suspensions (Fig. 3) that the aqueous concentration during
379 the active phase of the biodegradation of crystalline pyrene was three orders of magnitude higher
380 than the value of the K_m during uptake. Theoretically, an increase in exposure concentration caused
381 by solubilization did not result in enhanced uptake and biodegradation. The increased
382 mineralization rate in the presence of the rhamnolipid can be attributed to an additional passive
383 contaminant flow toward bacterial cells that were exposed to very high concentrations of dissolved
384 pyrene. This mechanism would be analogous to the carrier effect described for humic acids, which
385 enhances the biodegradation of crystalline and PDMS-associated pyrene (Tejeda-Agredano et al.,

386 2014) and crystalline phenanthrene (Smith et al., 2009) through an increased diffusion of the
387 contaminant to the bacterial cells, driven by an active rate of biodegradation. Dissolved organic
388 matter (DOM), such as humic acids, forms micelle-like structures similar to those formed by the
389 biosurfactants, into which PAHs may sorb for consumption by bacteria. However, the solubilization
390 caused by DOM may reach more moderate levels than those induced by the rhamnolipid due to the
391 structural arrangement of DOM macromolecules that hinders PAH access to the hydrophobic
392 regions (Wu et al., 2010). For this reason, the enhanced mineralization rate in the presence of DOM
393 is strictly dependent on an optimal range of concentrations (Haftka et al., 2008; Tejeda-Agredano et
394 al., 2014). This mechanism is caused by the diffusion of solubilized pyrene and confirms two other
395 PAH uptake mechanisms by bacterial cells, i.e., passive diffusion and active, energy-dependent
396 acquisition. For example, inhibitors of active transport prevented the active uptake of phenanthrene
397 by *Mycobacterium* sp. RJII-135 cells but not the passive diffusion uptake (Miyata et al., 2004).
398 Additionally, when *Mycobacterium gilvum* VM552 cells were exposed to high and low oxygen
399 tensions, the pyrene uptake shifted from first-order to linear-based kinetics. This indicated the
400 existence of these two different pyrene uptake pathways (Ortega-Calvo and Gschwend, 2010).
401 The proposed rhamnolipid-enhanced mechanism for the biodegradation of crystalline pyrene
402 seems to contradict the observed biodegradation results when pyrene was provided by partitioning
403 from PDMS. The rhamnolipid significantly enhanced the partitioning but did not result in a higher
404 biodegradation rate. The concentrations caused by rhamnolipid-enhanced partitioning, which were
405 significantly lower than with solid pyrene, may not have been sufficient to create a carrier effect for
406 bacterial cells. Alternatively, the results from bacterial attachment experiments indicate that the
407 influence of the rhamnolipid on attachment may be relevant in the PDMS system. On the one hand,
408 the high number of bacterial cells attached to PDMS in the absence of the rhamnolipid indicates that
409 a substantial fraction of the bacterial population was likely operating at exposure concentrations
410 higher than those estimated in the bulk aqueous phase by the solubilization experiments. This would

411 have positively influenced the mineralization rates observed with PDMS in an analogous way as the
412 exposure to spatial gradients of vapor-phase and NAPL-associated PAHs (Hanzel et al., 2012;
413 Ortega-Calvo and Alexander, 1994; Tejeda-Agredano et al., 2011). On the other hand, the
414 rhamnolipid caused a significant decrease in the number of cells attached to the PDMS surface and
415 negatively impacted the transformation. We hypothesize that the inhibited bacterial attachment and
416 the limited effect on solubilization relative to that observed for crystalline pyrene were the likely
417 causes for the absence of any enhancement in biodegradation in this exposure scenario.

418 Our results with PDMS differ from other studies; the balance between the two competing
419 mechanisms of enhanced solubilization and inhibition of cell attachment showed contrasting
420 impacts on the biodegradation of PAHs. For example, the surfactant Triton X-100 both decreased
421 and increased the biodegradation rate of naphthalene in di(2-ethylhexyl)phthalate (DEHP) and in
422 heptamethylnonane (HMN), respectively (Ortega-Calvo and Alexander, 1994). The surfactant
423 decreased the mineralization of naphthalene in DEHP because it did not enhance the partitioning
424 and prevented cell adhesion to the DEHP/water interface. However, the increased biodegradation
425 rate in HMN was caused by an increased partitioning rate that surpassed the inhibition of cell
426 adhesion. Another dual effect was reported for humic acids. Humic acids enhanced the
427 biodegradation of crystalline pyrene through solubilization but inhibited the biodegradation of
428 PDMS-associated pyrene as a result of decreased adhesion to the silicone surface (Tejeda-Agredano
429 et al., 2014). The present study showed that rhamnolipids can have multiple effects on the microbial
430 uptake and biodegradation of PAHs. The results of this study may provide new applications for the
431 optimized use of biosurfactants in bioremediation.

432

433 **Acknowledgements**

434

435 Support for this research was provided by the Spanish Ministry of Science and Innovation
436 (CGL2010-22068-C02-01 and CGL2013-44554-R), the Andalusian Government (RNM 2337) and
437 the FPI Programme (E.C.).
438

References

Accardi-Dey, A., Gschwend, P.M., 2002. Assessing the combined roles of natural organic matter and black carbon as sorbents in sediments. Environ. Sci. Technol. 36, 21-29.

Banat, I.M., Franzetti, A., Gandolfi, I., Bestetti, G., Martinotti, M.G., Fracchia, L., Smyth, T.J., Marchant, R., 2010. Microbial biosurfactants production, applications and future potential. Appl. Microbiol. Biotechnol. 87, 427-444.

Bueno-Montes, M., Springael, D., Ortega-Calvo, J.J., 2011. Effect of a non-ionic surfactant on biodegradation of slowly desorbing PAHs in contaminated soils. Environ. Sci. Technol. 45, 3019-3026.

Congiu, E., Ortega-Calvo, J.-J., 2014. Role of desorption kinetics in the rhamnolipid-enhanced biodegradation of polycyclic aromatic hydrocarbons. Environ. Sci. Technol. 48, 10869-10877.

Cornelissen, G., Rigterink, H., Ferdinandy, M.M.A., Van Noort, P.C.M., 1998. Rapidly desorbing fractions of PAHs in contaminated sediments as a predictor of the extent of bioremediation. Environ. Sci. Technol. 32, 966-970.

Efroymson, R.A., Alexander, M., 1994. Role of partitioning in biodegradation of phenanthrene dissolved in nonaqueous-phase liquids. Environ. Sci. Technol. 28, 1172-1179.

Garcia-Junco, M., Gomez-Lahoz, C., Niqui-Arroyo, J.L., Ortega-Calvo, J.J., 2003. Biodegradation- and biosurfactant-enhanced partitioning of polycyclic aromatic hydrocarbons from nonaqueous-phase liquids. Environ. Sci. Technol. 37, 2988-2996.

Gomez-Lahoz, C., Ortega-Calvo, J.J., 2005. Effect of slow desorption on the kinetics of biodegradation of polycyclic aromatic hydrocarbons. Environ. Sci. Technol. 39, 8776-8783.

Guerin, W.F., Boyd, S.A., 1992. Differential bioavailability of soil-sorbed naphthalene to two bacterial species. Appl. Environ. Microbiol. 58, 1142-1152.

Haftka, J.J.H., Parsons, J.R., Govers, H.A.J., Ortega-Calvo, J.J., 2008. Enhanced kinetics of

464 solid-phase microextraction and biodegradation of polycyclic aromatic hydrocarbons in the
465 presence of dissolved organic matter. Environ. Toxicol. Chem. 27, 1526-1532.
466 Hanzel, J., Thullner, M., Harms, H., Wick, L.Y., 2012. Walking the tightrope of bioavailability:
467 growth dynamics of PAH degraders on vapour-phase PAH. Microb. Biotechnol. 5, 79-86.
468 Jimenez-Sanchez, C., Wick, L.Y., Cantos, M., Ortega-Calvo, J.J., 2015. Impact of dissolved organic
469 matter on bacterial tactic motility, attachment, and transport. Environ. Sci. Technol. 49,
470 4498−4505
471 Johnsen, A. R., Wick, L. Y., Harms, H., 2005. Principles of microbial PAH-degradation in soil.
472 Environ. Pollut. 133, 71-84.
473 Miyata, N., Iwahori, K., Foght, J.M., Gray, M.R., 2004. Saturable, energy dependent uptake of
474 phenanthrene in aqueous phase by *Mycobacterium* sp. strain RJGII-135. Appl. Environ.
475 Microbiol. 70, 363-369.
476 Nickzad, A., Deziel, E., 2014. The involvement of rhamnolipids in microbial cell adhesion and
477 biofilm development - an approach for control? Lett. Appl. Microbiol. 58, 447-453.
478 Ochoa-Loza, F.J., Noordman, W.H., Jannsen, D.B., Brusseau, M.L. , 2007. Effect of clays, metal
479 oxides, and organic matter on rhamnolipid biosurfactant sorption by soil. Chemosphere 66,
480 1634-1642.
481 Ortega-Calvo, J.-J., Gschwend, P.M., 2010. Influence of low oxygen tensions and sorption to
482 sediment black carbon on biodegradation of pyrene. Appl. Environ. Microbiol. 76, 4430-
483 4437.
484 Ortega-Calvo, J.J., Alexander, M., 1994. Roles of bacterial attachment and spontaneous partitioning
485 in the biodegradation of naphthalene initially present in nonaqueous-phase liquids. Appl.
486 Environ. Microbiol. 60, 2643-2646.
487 Ortega-Calvo, J.J., Tejeda-Agredano, M.C., Jimenez-Sanchez, C., Congiu, E., Sungthong, R.,
488 Niqui-Arroyo, J.L., Cantos, M., 2013. Is it possible to increase bioavailability but not

environmental risk of PAHs in bioremediation? J. Hazard. Mater. 261, 733– 745

Patra, D., Mishra, A.K., 2002. Recent developments in multi-component synchronous fluorescence scan analysis. Trends Anal. Chem. 21, 787-798.

Posada-Baquero, R., Ortega-Calvo, J.J., 2011. Recalcitrance of polycyclic aromatic hydrocarbons in soil contributes to background pollution. Environ. Pollut. 159, 3692-3699.

Rhodes, A. H., McAllister, L. E., Semple, K. T., 2010. Linking desorption kinetics to phenanthrene biodegradation in soil. Environ. Pollut. 158, 1348-1353.

Schlautman, M.A., Yim, S.B., Carraway, E.R., Lee, J.H., Herbert, B.E., 2004. Testing a surface tension-based model to predict the salting out of polycyclic aromatic hydrocarbons in model environmental solutions. Water Res. 38, 3331-3339.

Schwarzenbach, R.P., Gschwend, P.M., Imboden, D.M., 2003. Environmental Organic Chemistry, second edition. John Wiley & Sons, New Jersey.

Smith, K.E.C., Rein, A., Trapp, S., Mayer, P., Karlson, U.G., 2012. Dynamic Passive Dosing for Studying the Biotransformation of Hydrophobic Organic Chemicals: Microbial Degradation as an Example. Environ. Sci. Technol. 46, 4852-4860.

Stelmack, P.L., Gray, M.R., Pickard, M.A., 1999. Bacterial adhesion to soil contaminants in the presence of surfactants. Appl. Environ. Microbiol. 65, 163-168.

Tejeda-Agredano, M.C., Gallego, S., Niqui-Arroyo, J.L., Vila, J., Grifoll, M., Ortega-Calvo, J.J., 2011. Effect of interface fertilization on biodegradation of polycyclic aromatic hydrocarbons present in nonaqueous-phase liquids. Environ. Sci. Technol. 45, 1074-1081

Tejeda-Agredano, M.C., Mayer, P., Ortega-Calvo, J.J., 2014. The effect of humic acids on biodegradation of polycyclic aromatic hydrocarbons depends on the exposure regime. Environ. Pollut. 184, 435-442.

Yang, Y., Zhang, N., Xue, M., Lu, S.T., Tao, S., 2011. Effects of soil organic matter on the development of the microbial polycyclic aromatic hydrocarbons (PAHs) degradation

potentials. Environmental Pollution 159, 591-595.

Wu, W., Sun, H., Wang, L., Li, K., Wang, L., 2010. Comparative study on the micelle properties of synthetic and dissolved organic matters. J. Hazard. Mater. 174, 635-640.

Zhang, Y., Maier, W.J., Miller, R.M., 1997. Effect of rhamnolipids on the dissolution, bioavailability, and biodegradation of phenanthrene. Environ. Sci. Technol. 31, 2211-2217.

Zhu, H., Aitken, M.D., 2010. Surfactant-enhanced desorption and biodegradation of polycyclic aromatic hydrocarbons in contaminated soil. Environ. Sci. Technol. 44, 7260-7265.

Table 1

Effect of rhamnolipid (400 mg/L) on phase exchange and mineralization of pyrene under bioavailability restrictions[a,b]

Scenarios[c]	Total concentration (μg/mL)	Phase exchange				Mineralization rate (ng/mL/h)	
		Rate (ng/mL/h)[d]		C_{eq} (ng/mL)[d]			
		Control	Rhamnolipid	Control	Rhamnolipid	Control	Rhamnolipid
Crystalline	5	190.0 ± 59.4 A	1386.1 ± 302.8 B	240.5 ± 11.1 A	2167.9 ± 152.7 B	16.8 ± 5.3 A	41.2 ± 7.1 B
PDMS	5	30.1 ± 5.2 A	97.9 ± 23.7 B	33.5 ± 0.9 A	126.8 ± 5.6 B	11.3 ± 2.9 A	8.9 ± 2.7 A
Soil	$4.2\ 10^{-3}$	0.7 ± 0.0[e]	ND[f]	0.5 ± 0.0[e,g] A	2.4 ± 0.1[g] B	0.1 ± 0.0[e] A	0.3 ± 0.0[e] B

[a] Errors are standard deviation of duplicate experiments. Statistical comparisons were performed with Student's t-test at P = 0.05.

[b] Values in a row followed by the same capital letter are not significantly different ($P \leq 0.05$).

[c] Crystalline, PDMS and soil indicate, respectively, that pyrene was provided as crystals, dissolved into polydimethylsiloxane (PDMS) or sorbed to soil.

[d] Values refer to the chemical present in the aqueous phase as determined by synchronous fluorescence spectrophotometry and equation 2.

[e] Standard deviation lower than 0.1.

[f] ND, not determined.

[g] Concentration of pyrene in the aqueous phase after 24 h in solubilization experiments.

Figure legends

Fig. 1. Dissolution of pyrene as crystals (A) and dissolved onto polydimethylsiloxane (B). The concentration of pyrene was measured with synchronous fluorescence spectrophotometry without (squares) and with 400 mg/L of rhamnolipid (circles). The dashed and solid lines represent the experimental fit to Equation 2 with and without the rhamnolipid, respectively. Error bars indicate the standard deviation of duplicate or triplicate measurements. When no error bars are visible, they are hidden by data points.

Fig. 2. Effect of rhamnolipid (400 mg/L) on the mineralization of pyrene under bioavailability restrictions: A) pyrene supplied as crystals (5 μg/mL), B) pyrene supplied by partitioning from loaded polydimethylsiloxane (5 μg/mL), C) as pyrene (4.2 ng/mL) sorbed to 800 mg/L of soil. Symbols indicate mineralization without (black squares) and with biosurfactant (white circles). The solid line represents the predictions from Equation 3 (A and B) or Equation 1 (C). Error bars indicate the standard deviation of duplicate experiments. When no error bars are visible, they are hidden by data points.

Fig. 3. Evolution of pyrene concentration in the presence of the rhamnolipid during biodegradation of crystalline pyrene (black squares). The results from the abiotic dissolution experiment with synchronous fluorescence spectrophotometry (white circles) and the mineralization experiment (white squares) in the same conditions are included for comparison. Error bars indicate the standard deviation of duplicate or triplicate measurements. When no error bars are visible, they are hidden by data points.

FIGURE 1

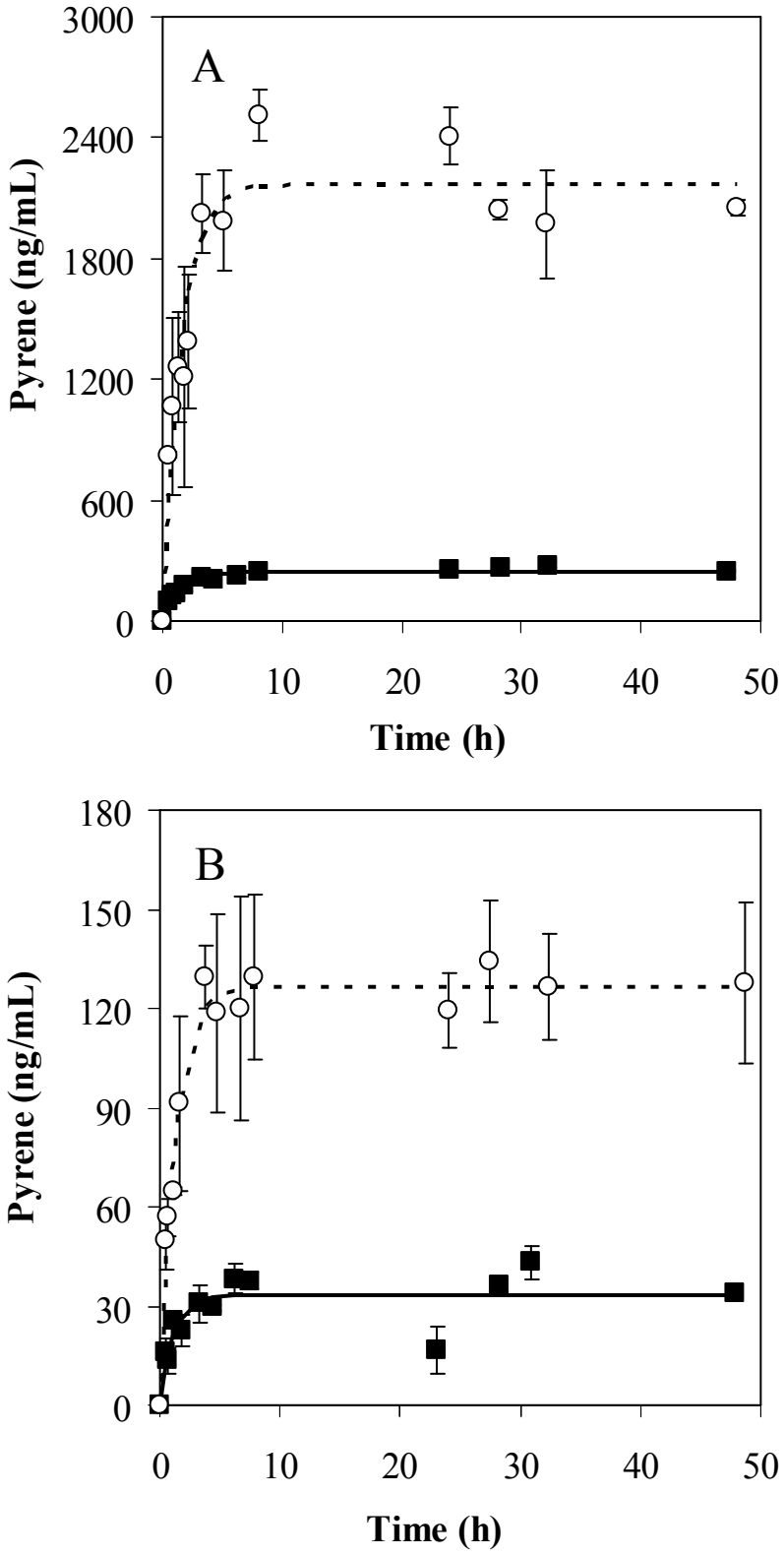
A
Pyrene (ng/mL)
3000
2400
1800
1200
600
0
0
10
20
30
40
50
Time (h)
B
Pyrene (ng/mL)
180
150
120
90
60
30
0
0
10
20
30
40
50
Time (h)

FIGURE 2

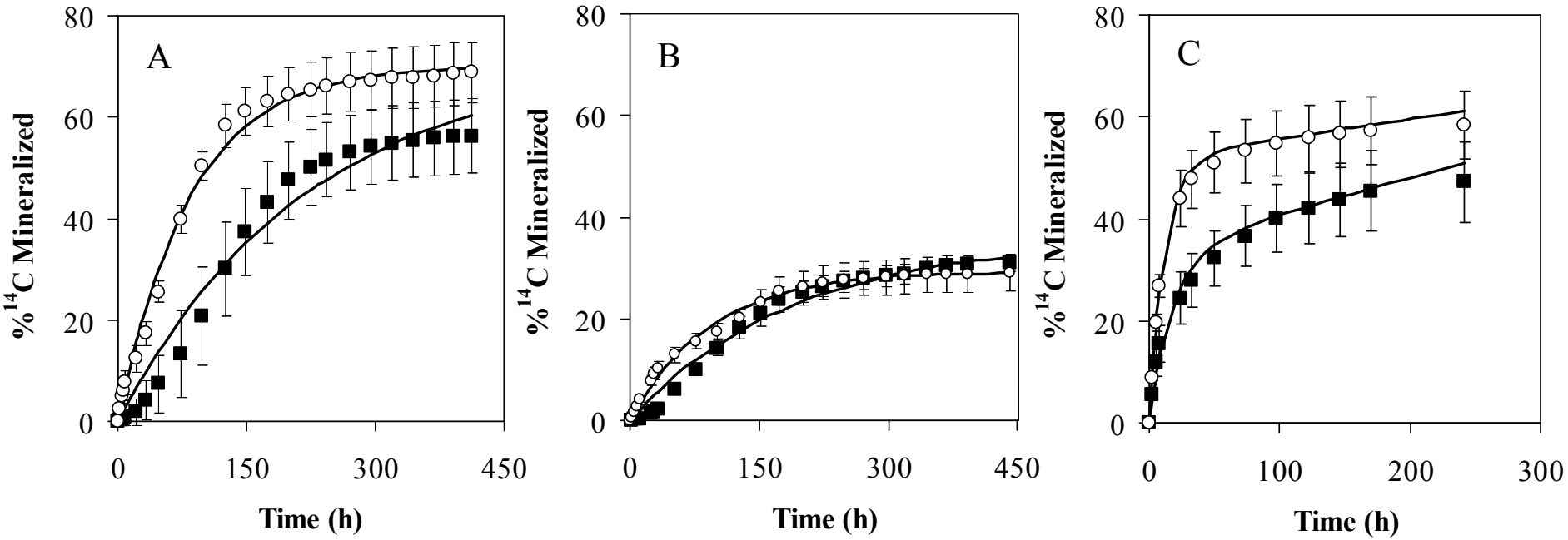

FIGURE 3

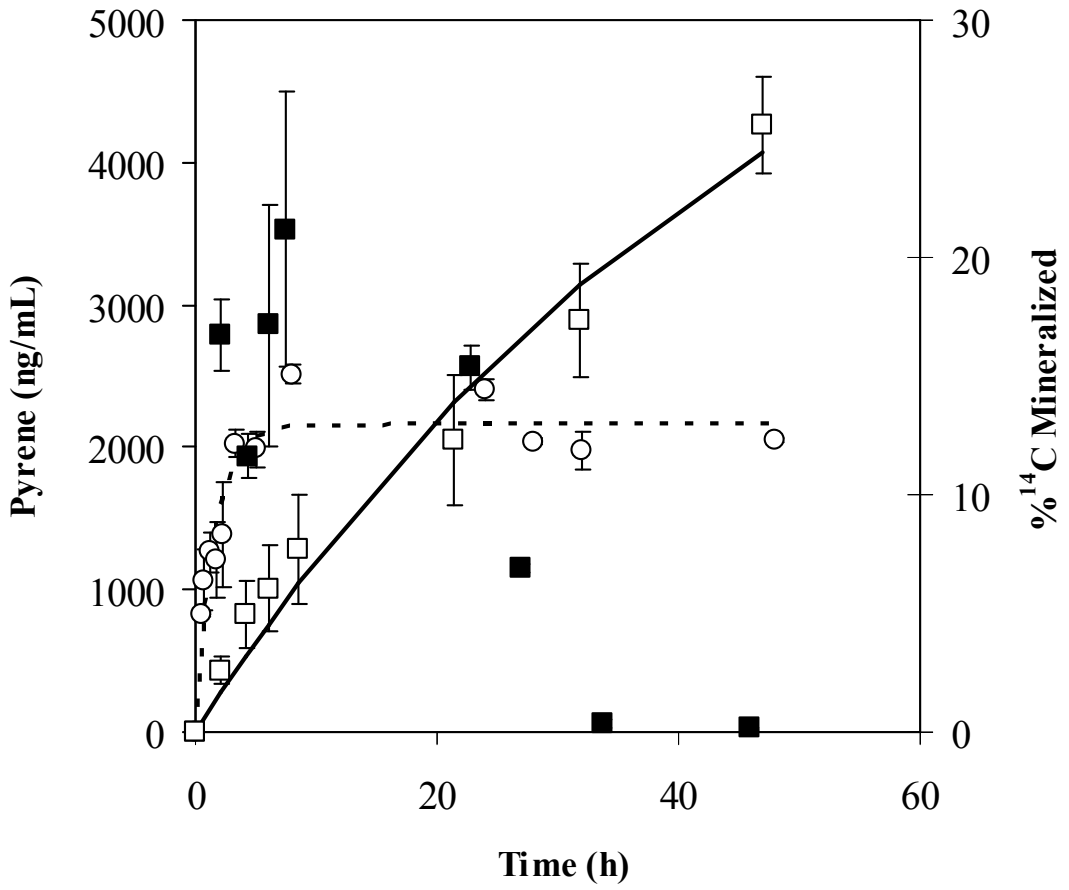
5000
4000
3000
2000
1000
0
Pyrene (ng/mL)
30
20
10
0
% 14C Mineralized
0
20
40
60
Time (h)